Water Resources Research

RESEARCH ARTICLE
10.1029/2018WR022827

An Entrogram-Based Approach to Describe Spatial Heterogeneity With Applications to Solute Transport in Porous Media

Marco Bianchi[1] **and Daniele Pedretti**[2]

[1]British Geological Survey (BGS), Nottingham, UK, [2]Geological Survey of Finland (GTK), Espoo, Finland

Key Points:
- Definition of entrogram and entropic scale to complement the geological entropy approach
- The entropic scale controls solute transport in a range of heterogeneous conductivity fields
- Entrogram explains the different impacts of structure on transport in 2-D and 3-D systems

Supporting Information:
- Supporting Information S1

Correspondence to:
M. Bianchi,
marcob@bgs.ac.uk

Citation:
Bianchi, M., & Pedretti, D. (2018). An entrogram-based approach to describe spatial heterogeneity with applications to solute transport in porous media. *Water Resources Research*, *54*, 4432–4448. https://doi.org/10.1029/2018WR022827

Received 22 FEB 2018
Accepted 2 JUN 2018
Accepted article online 8 JUN 2018
Published online 4 JUL 2018

Abstract The recently introduced geological entropy concept evaluates spatial order/disorder in the structure of the hydraulic conductivity (K) field to explain and predict certain characteristics of transport behavior. This concept is expanded in this work by introducing a novel tool for spatial analysis called *entrogram* from which a metric called *entropic scale* (H_S) can be calculated to measure the overall persistency of patterns of spatial association in a distributed field and to allow robust comparisons between different spatial structures. The entrogram and the entropic scale concepts are applied here to investigate the link between solute transport behavior and the spatial structure of K fields modeled as the distribution of three hydrofacies in alluvial aquifers. Accurate empirical relationships are found between H_S and key transport quantities confirming the clear correlation between transport and the structure of the K field described in terms of its entropic scale. The entrogram analysis is also applied to continuous 2-D and 3-D fields having identical lognormal K distributions, but with different connectivity. Comparisons between the entrograms and the calculated H_S values for these fields, as well as for their corresponding flow velocity distributions, shed light on the key differences among these structures in 2-D and in 3-D, which in turn explain their dissimilar impact on solute transport. The entrogram-based interpretation of the transport simulations seems to confirm that the geological entropy is a promising approach for predicting solute transport behavior simply from a description of the K field heterogeneity.

1. Introduction

In hydrogeology, upscaling is the process by which the scale of measurement of a certain variable is mathematically adapted to the required scale of interest for a model-based analysis (e.g., de Marsily et al., 2005; Wen & Gómez-Hernández, 1996). A variety of upscaling methods have been presented for flow and solute transport processes, from surrogate and proxy models (Asher et al., 2015; Fiori et al., 2015; Neuman & Tartakovsky, 2009) to approaches explicitly describing the spatial heterogeneity of the hydraulic conductivity (K) fields (e.g., Fogg & Zhang, 2016; Sanchez-Vila & Fernàndez-Garcia, 2016). Two main approaches based on effective descriptions of the K field have been traditionally followed for solute transport upscaling.

The first approach is at the basis of the traditional theories of stochastic hydrogeology and adopts multivariate normal (MVN; or multi-Gaussian) representations of the log-transformed K ($\ln K$) field. Stochastic theories are assumed to develop relationships between the hydrodynamic dispersion coefficients in the advection-dispersion equation and statistics (i.e., the mean K_G, the variance $\sigma^2_{\ln K}$, and the integral scale I) of the $\ln K$ field (Dagan, 1989; de Marsily, 1986; Gelhar, 1993; Neuman et al., 1987; Rubin, 2003). The general applicability of these relationships has been challenged by several studies (Adams & Gelhar, 1992; Cortis & Berkowitz, 2004; Gómez-Hernández & Wen, 1998; Lee et al., 2007; Liu et al., 2004; Molinari et al., 2015; Sánchez-Vila et al., 1996; Tompson et al., 1998; Wen & Gómez-Hernández, 1998; Zheng et al., 2011; Zheng & Gorelick, 2003; Zinn & Harvey, 2003), showing that the stochastic approach may be especially questionable in highly heterogeneous aquifers in which the K field structure is characterized by connected features of extreme values. This type of structure cannot be adequately represented by a MVN field (Journel & Deutsch, 1993), as connected features exert a strong control on groundwater flow and transport behavior in alluvial systems (Anderson, 1989; Bianchi et al., 2011; Bianchi & Zheng, 2016; Davies & Gibling, 2011; de Marsily et al., 2005; Dell'Arciprete et al., 2014; Fogg, 1986; Fogg et al., 2000; Fogg & Zhang, 2016; Weissmann et al., 1999).

The concept of connectivity has then emerged as a second approach to link transport behavior to the heterogeneity of the K field. Measures of connectivity (see review by Renard & Allard, 2013) include both "static" (i.e., those based on the physical properties of the media) and "dynamic" metrics (i.e., those based on metrics describing flow and transport processes). A series of static and dynamic connectivity metrics have been proposed (Fernàndez-Garcia et al., 2010; Fiori, 2014; Fiori & Jankovic, 2012; Freixas et al., 2017; Knudby & Carrera, 2005; Renard & Allard, 2013; Trinchero et al., 2008; Tyukhova & Willmann, 2016a, 2016b; Willmann et al., 2008). In the recent work of Rizzo and de Barros (2017), for instance, the connectivity of the K field is quantified with a static metric based on the identification of paths of least resistance (Tyukhova & Willmann, 2016a), which is subsequently shown to be correlated to the early arrival times of a solute plume. Connectivity is closely related to the concepts of percolation and critical path analysis (e.g., Harter, 2005; Hunt & Sahimi, 2017; Stauffer & Aharony, 1994). For instance, by invoking the percolation threshold, Knudby and Carrera (2006) associated the transmissivity along the paths of least resistance (critical path transmissivity) to the effective transmissivity of heterogeneous fields. In spite of the development of a large number of connectivity-based upscaling solutions, the correlation between connectivity metrics and measurable properties of flow and transport behavior remains in most cases not fully understood, limiting their applications for predictive purposes.

In recognition of these limitations, Bianchi and Pedretti (2017) introduced an alternative approach based on the assumption that solute transport behavior is sensitive to the degree of spatial order/disorder in the structure of the K field. This approach is called *geological entropy*, and a metric (i.e., the relative entropy index, H_R) based on information entropy concepts (Shannon, 1948) was proposed to quantify the degree of spatial disorder. Because the Shannon entropy H can be seen as a measure of unpredictability, it has been extensively applied to quantify uncertainty, disorder, and randomness in a wide range of disciplines, including hydrogeology, geostatistics, and related fields (e.g., Chiogna et al., 2012; Journel & Deutsch, 1993; Kitanidis, 1994; Mays et al., 2002; Ye et al., 2017). In Bianchi and Pedretti (2017), numerical simulations of solute transport in generic alluvial aquifers with a wide range of heterogeneity ($\sigma^2_{\ln K}$ between 1.7 and 28.0, mean lengths of the facies between 1 and 30 m) were performed to analyze the effect of spatial disorder on the first three spatial central temporal moments of the breakthrough curves (BTCs). Empirical expressions were subsequently developed to describe the correlation between H_R and these moments. One of these empirical expressions provided accurate predictions of the skewness (i.e., the degree of tailing) of the BTCs, suggesting that the geological entropy approach can effectively predict the occurrence of tailing from information about the K field heterogeneity.

The potential limitations of the relative entropy index H_R as defined in Bianchi and Pedretti (2017) are that it measures spatial disorder in a distributed field only at the local scale and that the choice of such scale could be subjective. These limitations can be addressed by means of a new tool for analysis that allows investigating spatial disorder or H_R at all the scales within the domain of interest. However, because it is reasonable to assume that different spatial distributions display distinctive patterns of spatial disorder at different scales, a new general unit of geological entropy is also needed for making robust comparisons.

The purpose of this paper is twofold. First, we extend the local-based geological entropy approach by introducing a new tool for spatial analysis called *entrogram* and, by its integration, a global metric of spatial order called *entropic scale* (H_S). As we did for the relative entropy index H_R, in this work we will also investigate the correlation between H_S and certain quantifiable characteristics of the transport behavior. The second purpose is to apply entrogram and entropic scale to explain the main conclusion of the recent study by Jankovic et al. (2017), in which exceptionally detailed simulations of solute transport were performed in 3-D K fields with different patterns of connectivity in the extreme values (high and low). In a previous and very influential study, Zinn and Harvey (2003) conducted a similar analysis in 2-D, which showed that the BTCs and in general transport behavior are significantly impacted by the differently connected structures. Contrary to the conclusions of Zinn and Harvey (2003), the main finding of Jankovic et al. (2017) is that the BTCs calculated in the different fields are surprisingly similar. This result was interpreted as the indication of a "universal" transport behavior independent from the structure of the K field, which can be predicted only from knowledge of its first-order statistical parameters (e.g., Fiori et al., 2017). In this work, we will explain the results between Zinn and Harvey (2003) and Jankovic et al. (2017) through the application of the geological entropy approach, in particular by measuring, comparing, and analyzing the entropic scales of the different 2-D and 3-D fields and the resulting transport characteristics.

2. Theoretical Background

2.1. The Concept of Geological Entropy

The concept of geological entropy developed in Bianchi and Pedretti (2017) consists of quantifying the degree of spatial disorder (or alternatively the opposite, i.e., order) in the structure of the K field to gain key information for the interpretation and prediction of transport behavior in heterogeneous media. This quantification is based on the application of the information entropy concepts originally proposed by Shannon (1948) to measure the average amount of information required to predict the outcome of a random process. For a generic random process generating a discrete number of n outcomes with probabilities $p_1, p_2, \ldots, p_n$, the Shannon entropy H can be written as follows:

$$H = -\sum_{i=1}^{n} p_i[\ln p_i] \tag{1}$$

H is equal to zero when there is low uncertainty about the process ($p_i = 1, p_{j \neq i} = 0$), while it is maximum ($H = \ln n$) when all the outcomes have equal probability ($p_i = 1/n$).

In Bianchi and Pedretti (2017), equation (1) was applied to calculate the local and global entropies of the spatial distribution of a categorical random variable F defined over a grid covering a certain domain of interest. In particular, the *global* entropy H_G of F was defined as follows:

$$H_G = -\sum_{i=1}^{N} p_{G,i}\left[\ln p_{G,i}\right] \tag{2}$$

where $p_{G,\,i}$ is the volumetric fraction (i.e., the probability of occurrence) of a certain category i over the domain of interest and N is the total number of categories of F. Entropy calculations based on equation (2) can be extended to continuous variables by binning (discretizing) the continuous distribution into classes. However, the loss of information due to discretization needs to be carefully evaluated as we will discuss later.

For each block of the grid used to discretize the spatial distribution of F, the *local* entropy H_L can also be defined:

$$H_L(\mathbf{l}) = -\sum_{i=1}^{N} p_{L,i}(\mathbf{l})\left[\ln p_{L,i}(\mathbf{l})\right] \tag{3}$$

where $p_{L,\,i}(\mathbf{l})$ are the local volumetric fractions (i.e., marginal probabilities of occurrence) of the categories of F within a subdomain whose dimensions are defined by the vector $\mathbf{l} = l_x\mathbf{i} + l_y\mathbf{j} + l_z\mathbf{k}$. The scalar components l_x, l_y, and l_z are equal to the half-lengths of the subdomains (centered around the grid block) considered for the local entropy calculation along the Cartesian directions x, y, and z.

2.2. Entrogram Analysis and Entropic Scale Estimation for Categorical Fields

From equation (3), a relative entropy index $H_R(\mathbf{l})'$ is defined for each grid block and each subdomain defined by l as follows:

$$H_R(\mathbf{l})' = \frac{H_L(\mathbf{l})}{H_G} \tag{4}$$

The relative entropy index provides a measure of spatial disorder. In particular, low values suggest an orderly structure in which one or a small number of categories of F is more frequent than others at the scale of the subdomains defined by l. Conversely, higher values suggest disorderly structures in which the local and the global entropy values tend to be similar because all the categories of F are more or less equally frequent within the subdomains.

In Bianchi and Pedretti (2017), the local entropy H_L and therefore the relative entropy index H_R were evaluated at the local scale only and specifically within a subdomain of half-lengths equal to 1.5 grid blocks in each direction. In this work, the evaluation of H_R is extended to all the possible subdomains with half-lengths larger than 0.5 grid blocks within the domain of interests. In particular, for a set of half-lengths (l_x, l_y, l_z), a number of random locations are selected within the domain using a quasi-random discrepancy sequence (Sobol LPτ), and a population of $H_R(\mathbf{l})'$ values is calculated for each location. This calculation is repeated for different sets of half-lengths until the dimensions of the subdomains become comparable to those of the entire domain. By plotting the average values of the populations of $H_R(\mathbf{l})'$ for the different sets of half-lengths against the

subdomain dimensions, a variogram-like graph called *entrogram* is produced, which allows to explore the behavior of the relative entropy index H_R at different scales. Naimi (2015) introduced the term entrogram for the quantification of the spatial association of both continuous and categorical geographical variables and presented applications to a digital elevation model and a land cover map. Although the definition of the entrogram in this work is very different, we decided to maintain the same terminology used by Naimi (2015) given that both graphs have a variogram-like shape and they are both based on information entropy concepts. When equal half-lengths are considered along the Cartesian directions (i.e., $l_x = l_y = l_z$), the omnidirectional experimental entrogram can be defined as follows:

$$H_R(l) = \frac{1}{n_s(l)} \sum_{i=1}^{n_s} H_{R,i}(l) \tag{5}$$

where $H_{R,i}(l)$ is the relative entropy index calculated for the i-subdomain of half-length equal to l and n_s is the number of subdomains for which the local entropy H_L is evaluated. This number, which belongs to the interval [0, 1], depends on l given that a lower n_s is required for a robust estimation of the average H_R as the dimensions of the subdomain increase. Similar to the way the classic (semi) variogram or the covariance function of a random function describes the variability of spatial correlation with distance (Isaaks & Srivastava, 1990), the entrogram describes the variability of spatial disorder in a discretized field. Moreover, both the entrogram and certain standard variogram models (i.e., the exponential, Gaussian, and the spherical model) tend to increase monotonically with distance until they reach an asymptotic value. For the entrogram, this value is $H_R(l) = 1$, that is, when the local entropy H_L equals the global entropy H_G.

2.3. Illustrative Example

An illustrative example of the information that can be drawn from the analysis of the entrograms for different fields is presented in Figure 1, where we show three spatial distributions (A, B, and C) of a generic binary variable F discretized over a regular 50×50 grid. The three distributions were generated using a Boolean simulation code (Deutsch & Journel, 1998), which randomly places ellipsoids (shown in white in Figure 1) of different sizes until a target volumetric fraction is met (i.e., 0.6 for all the structures). For the field A, the radii of the ellipsoids in both Cartesian directions are equal to one grid block, and therefore, the spatial distribution of F is very chaotic and disorderly at all scales. This is reflected in a very steep increase of the entrogram calculated for this field, which starts at a value of $H_R = 0.9$ for a length of only 1.5 grid blocks and rapidly reaches the $H_R = 1.0$ asymptote. On average, $H_R > 0.95$ is calculated for subdomains with l equal to only two grid blocks, correctly indicating the lack of an organized structure. Intuitively, one shall expect that the structure of F becomes more organized as the size of the ellipsoids increases due to the increment in spatial continuity of these features. This is indeed the case for structures B (radius = 2 blocks) and C (radius = 8 blocks), and it is correctly reflected by the entrograms of these two structures. In particular, H_R values for structure B start at about $H_R = 0.6$ for a length of 1.5 block and increase monotonically until they reach the asymptote for subdomains with $l > 13$ blocks. The most organized and orderly structure (structure C) is characterized by the smoothest increment in entropy. This entrogram starts at a value of about $H_R = 0.15$ while $H_R > 0.95$ are calculated only for large subdomains comparable to the entire domain.

2.4. Entropic Scale Calculation

The qualitative considerations drawn from the analysis of the entrogram can be summarized by calculating the integral of the entrogram to obtain a metric called *entropic scale*. Given an omnidirectional entrogram $H_R(l)$, the entropic scale (H_S) is defined by the following:

$$H_S = \int_0^\infty [1 - H_R(l)]\mathrm{d}l \tag{6}$$

To a certain extent, the concept of the entropic scale is similar to that of the integral scale of a covariance function for a spatial random variable. In fact, they are both measures of spatial persistence. However, while the integral scale measures the persistence of correlation of a spatial random variable (Rubin, 2003), H_S can be seen as a measure of the persistence of clustering or in other terms of patterns of spatial association. Therefore, H_S can be used as a robust global metric of spatial order, like the CS3 indicator of static

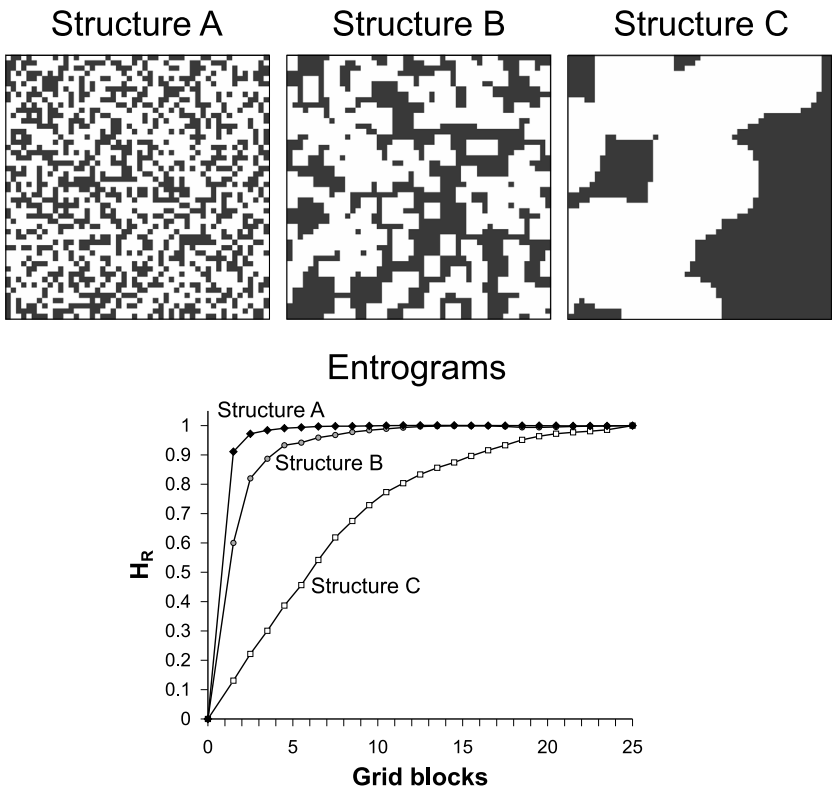

Figure 1. Entrogram comparison for binary systems with identical proportions for the two categories but with different spatial structures.

connectivity derived by Knudby and Carrera (2005). For instance, the H_S for the fields A, B, and C in Figure 1 are equal to 0.9, 1.8, and 7.2 grid blocks, respectively. These values, which were numerically evaluated using the trapezoidal method, correctly rank the degree of spatial order in the three structures (C more orderly than B and, in turn, B more orderly than A), while being also consistent with the lengths of the axes of the ellipsoids for each field.

We highlight two points of the proposed approach that need clarification. The first is that because the entropic scale is a global metric that takes into account the spatial structure of the entire field, it relies on the assumption of stationarity. This is a common assumption, for instance, in theoretical analyses of solute transport in heterogeneous media where the spatial distribution of *K* field is usually modeled as a stationary random variable. However, the assumption of stationarity especially for geological media is not always realistic (e.g., Rehfeldt et al., 1992) and practically difficult to test for field applications. Therefore, it remains a working hypothesis (Rubin & Seong, 1994). For nonstationary fields, the relative entropy indicator H_R calculated at a local scale (Bianchi & Pedretti, 2017) could then be a more appropriate measure of spatial disorder. The second point is that the calculation of the integral scale requires a discretized model of the spatial distribution of the property of interest. Therefore, the uncertainty in the estimated entropic scale depends on the model uncertainty, which originates from various sources including the data, the model parameters, and the model structure itself (e.g., Refsgaard et al., 2006). Nonetheless, the entrogram and the entropic scale can be calculated for any discretized spatial distribution regardless of the dimensionality or the modeling methodology (e.g., deterministic, stochastic, two-point, and multiple-point geostatistics).

3. Application of the Geological Entropy Approach

3.1. Categorical *K* Fields

One of the objectives of this work is to revisit the results of the analysis presented in Bianchi and Pedretti (2017) in light of the newly introduced entrogram analysis and entropic scale. In particular, similar to the previous study, we aim to develop empirical relationships between the entropic scale of the *K* field and certain

statistics of the BTC that can then be used as upscaled models to predict transport behavior without the need to solve the flow and solute transport equations. Putting this into practice requires three steps: (1) generation of the spatial distribution of K using a method of choice; (2) analysis of the geological entropy of the generated distribution using the entrogram and entropic scale calculation; and (3) predictions of the BTC statistic of interest using empirical relationships and calculated entropic scale.

The flow and transport modeling in this study as well as the methodology for generating the stochastic K fields are the same as those described by Bianchi and Pedretti (2017), to which we refer for details not reported hereafter. Briefly, six groups of synthetic K fields were generated in previous work from the distributions of three hydrofacies representing typical alluvial environments. These distributions were simulated with the transition probability/Markov Chain approach (Carle, 1999; Carle & Fogg, 1996). In the present work, we selected a group of K fields considering nine alluvial-like aquifers characterized by one highly permeable hydrofacies (volumetric fraction equal to 0.2), representing mostly coarse grained sediments, embedded in a matrix of low K sediments (volumetric fraction equal to 0.6). A third hydrofacies is also considered to represent deposits with intermediate conductivity. Conductivity values are assigned to each hydrofacies resulting in a three-modal distribution shared by all the K fields with identical univariate $\sigma^2_{\ln K}$ equal to 7.3. Nonetheless, each field has a unique spatial structure (see Figure S2 in Bianchi & Pedretti, 2017) imposed by the horizontal mean length (L_h) assigned to the most permeable hydrofacies. These lengths vary between 1 and 30 m within the group.

Monte Carlo simulations of groundwater flow and solute transport were conducted for an ensemble of 100 realizations for each K field scenario. Flow was simulated with the finite-difference code MODFLOW-2005 (Harbaugh, 2005), using a grid with block size equal to 1 m × 1 m × 0.5 m, covering a 40-m-thick domain of area equal to 200 m × 300 m on the horizontal plane. Specified head boundary conditions were set to create uniform flow steady-state conditions. Conservative transport behavior in the flow fields was simulated with the particle-tracking code RW3D (Salamon et al., 2006). The cumulative distribution function (CDF) of the particle arrival times at a control plane located 250 m down-gradient the injection line was collected for each simulation and used for the ensemble-based stochastic transport analysis. All transport simulations embed advection, local mechanical dispersion, molecular diffusion, and homogeneous effective porosity (θ).

To characterize the transport behavior and investigate the link with the entropic scales of the K fields, we consider several statistics directly obtained from the arrival time CDFs. Similar to the approach described in Bianchi and Pedretti (2017), we first evaluate the median values of the ensemble of centered temporal moments (mean, variance, and skewness). In addition, in this work we extend the analysis to the median values of three percentiles of the arrival time CDFs. Two of the chosen percentiles (p = 0.05 and p = 0.95) describe the early- and late-time arrivals, while the third (p = 0.50) is simply the median of the arrival time distributions. An estimation of the early- and late-time arrivals is important in the context of groundwater remediation and health risk assessment to define the beginning of contamination at sensible receptors and the duration of contaminant exposure (e.g., de Barros et al., 2013; Maxwell et al., 2008).

3.2. Continuous K Fields

Numerical experiments of solute transport similar to those performed by Zinn and Harvey (2003) and Jankovic et al. (2017) are conducted in 2-D and 3-D domains in which the spatial distribution of K is modeled as a continuous lognormal stationary random function. The objective of this analysis is first to reproduce the results of the two previous studies and then to test whether the geological entropy approach and, in particular, the entrograms and entropic scales of these fields can explain the contrasting interpretations of transport behavior in the 2-D and the 3-D fields. In the following sections, we summarize the characteristics of the conductivity fields and the numerical simulations.

3.2.1. Conductivity Field Structures

Isotropic MVN ln$K$ fields (MVN fields) are generated with a sequential Gaussian simulation algorithm (Remy et al., 2009). We considered a Gaussian covariance function as in the original work of Zinn and Harvey (2003), noticing however that the MVN fields generated by Jankovic et al. (2017) were based on spherical and exponential models instead. The domain for geostatistical simulations is discretized with grids consisting of 65,536 regular blocks for 2-D fields and of more than 16,777,216 blocks for 3-D fields. For both 2-D and 3-D fields, the integral scale (I) of the Gaussian covariance function is equal to 8 blocks, and therefore, the lengths of the domain are equal to 32 I for each Cartesian direction. For each realization, the univariate distribution of ln$K$ has zero mean and variance $\sigma^2_{\ln K} = 8$, which is also consistent with the maximum variance considered in

the previous studies. Since the dimensions of our domain are about one third of those considered by Jankovic et al. (2017), we ensured operating under ergodic conditions by means of Monte Carlo simulations instead of a single-realization analysis. In particular, 100 realizations of the MVN fields are generated, and all the results reported hereafter including the entrograms, entropic scales, and simulated transport results are taken as the average of the ensemble of these realizations. A comparison between the results obtained from our Monte Carlo based approach and those obtained by Jankovic et al. (2017) is analyzed to gain confidence about the quality of our results and provide a solid comparison with their study.

For each realization of the MVN field, corresponding connected (CNT) and disconnected (DSC) structures are generated following the four-step procedure of Zinn and Harvey (2003). These steps transform a MVN field into a new field having the same univariate distribution of the original field but with different connectivity of the values on the left or on the right tail of the normal distribution. In particular, the CNT fields are characterized by connected structures of high-K values, while the DSC fields present disconnected high-K zones and connected patterns of low K. As already noted in Zinn and Harvey (2003) and Jankovic et al. (2017), the application of the transformation procedure to a MVN field results in a reduction of the original correlation length. For the fields considered in this work, the integral scales of the CNT and DSC fields (I') are 1.76 times smaller than the values of the MVN fields. This value is very similar to the factor equal to 1.86 calculated by Zinn and Harvey (2003) and somewhat different from the value of 2.94 for fields based on exponential covariance functions considered by Jankovic et al. (2017). We therefore tested the consistency of our analysis, by considering additional 3-D MVN fields based on an exponential covariance function. We estimated a factor of 2.74, which is similar to the one obtained by Jankovic et al. (2017). To take into account the reduction in integral scale from the original value of the MVN field based on a Gaussian covariance function, the dimensions of the blocks of the grid for the CNT and DSC fields were reduced by a factor $F = 1/1.76 = 0.59$ in each direction such that the ratio of eight blocks per integral scale I' and a domain length equal to $32I'$ in all the directions are maintained for these fields.

3.2.2. Numerical Simulations of Flow and Transport

Steady-state uniform groundwater flow in the generated heterogeneous K fields is solved using MODFLOW-2005. The dimensions of the blocks of the numerical grid are equivalent to those of the grid for the geostatistical simulations. Specified head boundary conditions are applied to the upstream and downstream boundaries of the domain, while no-flow conditions are applied to the remaining boundaries.

Conservative solute transport is simulated with the semi-analytical particle tracking code MODPATH (Pollock, 2016) based on a linear interpolation scheme of the flow velocities. The two previous studies of Zinn and Harvey (2003) and Jankovic et al. (2017) investigated the effect of molecular diffusion on transport behavior in the different structures. Accordingly, the simulations took into account different values of the Peclet number (Pe). The conclusions regarding the sensitivity of transport with respect to Pe are somewhat different between the two studies. According to Zinn and Harvey (2003), lower Pe values tend to mask the differences between the BTCs of the different K field structures, while the BTCs calculated by Jankovic et al. (2017) do not show significant changes with Pe. Because of these discrepancies, we decided to focus only on the case of purely advective transport ($Pe = \infty$) to avoid further complications in the interpretation of the results in light of the application of the geological entropy approach.

For 2-D transport simulations, 10^5 particles are injected instantaneously using a flux-weighted scheme along a line perpendicular to the mean flow direction. The injection line is located at a distance of 2 integral scales from the upstream boundary and is 26 integral scales long. The location at the center of the domain allows the presence of two buffer zones of width equal to 3 integral scales at each side for avoiding interferences between particle paths and the no-flow boundaries (Bellin et al., 1992). For 3-D simulations, the injection is also flux-weighted and extended along the vertical dimension; the particles are injected within a square with sides equal to 26 integral scales. For each type of K field structure, the ensemble of 100 distributions of particle arrival times were collected at the outflow boundary at a distance of 30 integral scales from the injection zone. The same statistics used for the analysis for the categorical K fields (section 2.2) are used to quantify the transport behavior in the continuous K fields.

Following Jankovic et al. (2017) based on Fiori et al. (2015), the accuracy of the numerical simulations is tested through comparisons between the mean advective velocity $\overline{U}$ calculated from the results of the transport simulations and the mean of the component of the Eulerian velocity field parallel to the mean flow

Table 1
Comparisons Between Metrics for the 2-D and 3D Structures

	2-D structures			3-D structures		
	MVN	CNT	DSC	MVN	CNT	DSC
H_S/I (K field)	0.78	0.92	0.92	0.52	0.66	0.66
H_S/I(U field)	0.90	1.13	1.14	0.54	0.71	0.72
$\overline{U}/U_{mean}$	0.94	0.99	0.97	0.93	0.96	0.95
K_{eff}/K_G	1.01	3.14	0.44	3.54	7.83	1.41
t_5 [tU_h/I]	7.8	2.0	27.4	1.4	0.8	5.1
t_{50} [tU_h/I]	18.9	5.5	57.0	4.8	2.0	16.4
t_{95} [tU_h/I]	71.7	25.4	130.7	22.2	10.5	47.0
t_5 [$t\overline{U}/I$]	8.5	6.5	12.6	5.5	6.5	7.6
t_{50} [$t\overline{U}/I$]	20.6	18.1	26.2	18.4	16.1	24.5
t_{95} [$t\overline{U}/I$]	78.2	84.1	60.0	84.9	86.2	70.4
Skewness	25.2	40.3	2.9	46.5	64.2	3.2

Note. MVN = multivariate normal; CNT = connected; DSC = disconnected.

direction (U_{mean}). In each simulation, the components of the Eulerian velocity field ($\mathbf{U} = \mathbf{q}/\theta$) are calculated assuming homogeneous effective θ and by averaging the specific discharge (q) across the numerical grid block interfaces. The accuracy of the numerical analysis is confirmed by the similarity in the ensemble mean values of the two mean velocities (i.e., $\overline{U}/U_{mean}$ between 0.93 and 0.99; Table 1). A further check on the accuracy of the flow simulations is provided by the calculation of the effective hydraulic conductivity (K_{eff}) for each structure. The calculated values (Table 1) are consistent with the previous numerical estimations (Jankovic et al., 2017; Zinn & Harvey, 2003) and some theoretical results (Matheron, 1967; Xavier Sanchez-Vila et al., 2006). A more detailed explanation of these criteria used to check the accuracy of the numerical simulations is presented in the supporting information (SI).

3.2.3. Entropic Scale Calculations for Continuous *K* and *U* Fields

The entrogram calculation (equation (5)) for a continuous variable requires that data are first binned into a number of classes. As done in other studies (e.g., Kang et al., 2017; Le Borgne et al., 2008), the K and U distributions are discretized into N classes of equal probability by initially defining $N + 1$ regularly spaced threshold values $\tau_i \in [0, 1]$ and then by calculating the quantiles $q(\tau_i)$ of the continuous data distribution. A given K (or U) value is finally assigned to a certain class C_i if $q(\tau_i) < K < q(\tau_{i+1})$.

Different values of N were tested in order to determine an optimal number of classes for the entrograms and entropic scale calculations. Some of the results of this analysis are presented in Figure S1 of the SI for one of the generated MVN fields. In general, the entropic scale of the K field tends to decrease rapidly from low N values, and then it stabilizes around a constant value for $N > 30$. The decrease in spatial order indicated by the behavior of the entropic scale is consistent with the progressively larger amount of spatial heterogeneity or information that is taken into account as the number of classes increases. Based on these results and the fact that the computational time required to calculate the entrogram increases with N, a value $N = 40$ is considered optimal for entrograms and entropic scale calculations of the generated continuous K fields.

4. Results and Discussion

4.1. Link Between Entropic Scale and Transport

We first analyze and discuss the results of the entrogram and entropic scale calculations applied to the group of categorical K fields. It is recalled that these have identical univariate distribution ($\sigma^2_{\ln K} = 7.3$), but different structures according to the mean lengths (L_h) in the horizontal plane assigned to the most permeable hydrofacies in the T-PROGS simulations. The shape of the calculated experimental entrograms (Figure 2a) allows ranking the fields in terms of spatial disorder in the structure. The higher spatial disorder in the structure of the K fields with shorter L_h is indicated by a sharp increase of H_R at shorter distances. Conversely, the entrograms for fields considering higher L_h values tend to reach the $H_R = 1$ asymptote at higher distances.

In Bianchi and Pedretti (2017), we used values of the entrogram at the first lag to quantify the spatial order of the different K fields and to make comparisons between different structures. We demonstrated that this approach is effective in ranking different structures at the local scale, and we were able to link this metric to some characteristics of transport. However, as shown in Figure 2a, the analysis of the entire entrogram allows a more comprehensive characterization of H_R at different distances and of the persistency of spatial order at different scales. For instance, H_R values in the order of 0.95 (high spatial disorder) are reached after just about three lags (distance = 4.5 m in Figure 2a) for the K field with $L_h = 1$ m and after about four lags (distance = 6 m) for the K field with $L_h = 2.5$ m. These distances indicate that these fields have structures where there is a 95% probability on average that all the three hydrofacies are represented with their respective global proportions within a distance of few lags from each point of the domain. Conversely, for more orderly structures and larger L_h values, the distances at which $H_R = 0.95$ are in the order of 20 to 30 m, meaning that one of the categories is more frequent than the others within distances of 10 to 15 m from each block.

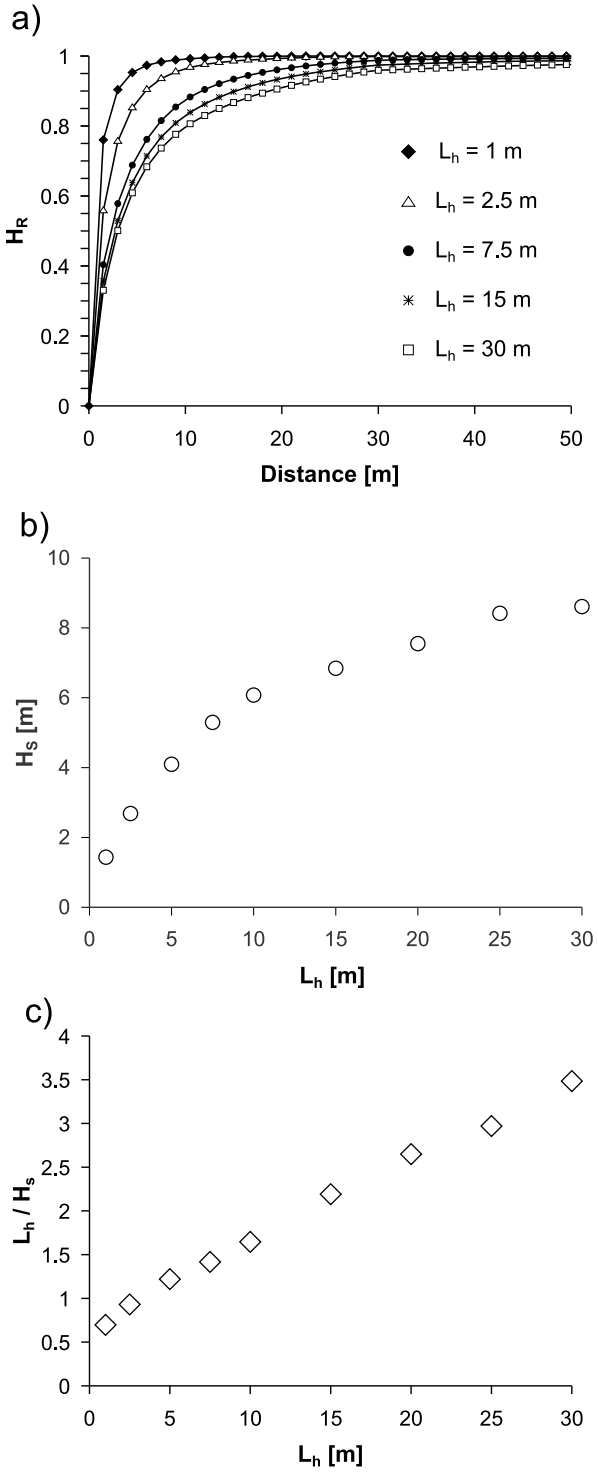

Figure 2. Entrograms (a), corresponding entropic scales (b), and plots of the ratio L_h/H_S (c) calculated for categorical K fields with different mean lengths (L_h).

A more quantitative and rigorous assessment of the degree of spatial order is provided by the values of H_S calculated by applying equation (6) to the entrograms of the K fields. The resulting values are in the range between 1.4 m for fields with L_h = 1 and 8.6 m for fields with L_h = 30. The behavior of the calculated H_S with L_h is nonlinear (Figure 2c) with a steep increase in H_S for $L_h < 10$ m followed by less accentuated increments for larger L_h values. A plot of the ratio L_h/H_S against L_h suggests instead a linear relationship between these two quantities for the considered categorical K fields (Figure 2c).

We now investigate the correlation between the calculated entropic scales and the results of the stochastic transport simulations. Median values of the statistics used to quantify transport behavior are plotted in Figure 3 as a function of the ratios L_h/H_S for the different fields. For all these statistics, the relationship between the calculated values m and the L_h/H_S ratio is best described by empirical power law functions in the following form:

$$m = a\left(\frac{L_h}{H_s}\right)^b + m_\infty \tag{7}$$

where the values of the parameter a, the exponent b, and the asymptotic value of the metric (m_∞) differ for each statistic (Table 1 in the SI). In particular, the exponent b is negative for every m except for the median skewness of the arrival time distributions. These relationships confirm the correlation between measurable quantities defining transport behavior and the degree of spatial order in the K field (Bianchi & Pedretti, 2017) and show that such correlation still holds when the degree of spatial order is expressed in terms of entropic scale H_S.

The clear correlation between L_h/H_S and the 5th (t_5) and 95th (t_{95}) percentiles (Figures 3e and 3f), respectively, supports our previous findings and reinforces the idea that geological entropy could be a very promising concept to be used for predicting transport in heterogeneous media. Previous studies have explained the earlier than expected arrival of solutes to the presence of preferential flow paths (Bianchi et al., 2011; Zheng & Gorelick, 2003) and connectivity of highly conductive sediments in alluvial aquifers (Knudby & Carrera, 2006; Wen & Gómez-Hernández, 1998; Willmann et al., 2008). However, only few formal relationships have been proposed between connectivity metrics and t_5 (Fiori & Jankovic, 2012; Rizzo & de Barros, 2017; Tyukhova & Willmann, 2016a). Late-time transport behavior has been related to mass transfer and diffusion processes through low conductive zones (LaBolle & Fogg, 2001), which have been modeled with non-Fickian transport approaches (Berkowitz et al., 2006; Haggerty & Gorelick, 1995; Neuman & Tartakovsky, 2009; Zhang et al., 2007). The correlations shown in Figure 3 indicate that the geological entropy approach based on the calculation of the entrogram and entropic scale can provide the necessary information to predict both early- and late-time arrivals in highly heterogeneous alluvial aquifers ($\sigma^2_{\ln K} \approx 8$) with realistic hydrofacies distributions. This is true provided that the empirical parameters of the correlation are known. Generalizing the results for universally scalable correlations and fully predictive upscaling are left open for future development.

A final observation of Figure 3 reveals that there could be a threshold above which the considered statistics (except for the skewness) cease to be dependent on the L_h/H_S ratio. For most of the considered fields, it seems that a value of $L_h/H_S \approx 1.5$ (shown by vertical dashed lines in Figure 3) can be a general measure to indicate the end of correlation between m and L_h/H_S, although the range of uncertainty from the visual

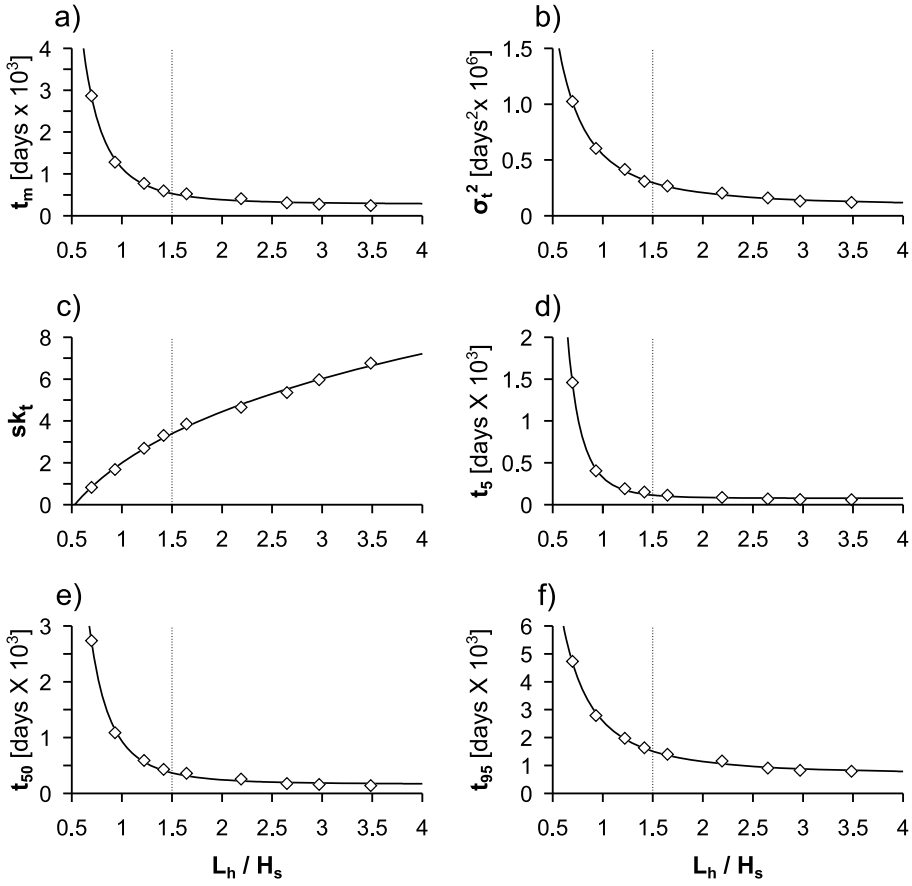

Figure 3. Median values of the statistics of the breakthrough curve calculated for the group of nine conductivity fields as a function of the ratio L_h/H_S. Mean (t_m), variance (σ_t^2), and skewness (sk_t) of the distribution of arrival times are presented in panels (a), (b), and (c), respectively. The 5th percentile (t_5), the median (t_{50}), and the 95th percentile (t_{95}) are shown in (c), (d), and (e), respectively. Solid lines indicate the best-fitted power law expressions (equation (7)).

assessment seems to indicate a fluctuation in the order of ±0.5. In other words, when L_h is more than 1.5 times larger than the entropic scale of the field, the statistics of the arrival time distributions for the different structures tend to be very similar (m_∞). Even for the skewness (sk_t), which increases monotonically with the ratio L_h/H_S, the value of 1.5 seems to separate the initial part of the curve where the relationship between sk_t and L_h/H_S is strongly nonlinear from the second part where sk_t increases almost linearly with L_h/H_S (Figure 3c). Recalling that the calculated values of H_S tend to become more and more similar as L_h increases, the fact that the statistics tend to their respective m_∞ values for $L_h/H_S > 1.5$ seems to suggest that transport behavior is more affected by the entropic scales of the different fields rather than by the mean lengths of the high-K hydrofacies. Moreover, if we assume L_h as a measure of spatial correlation similar to the ranges of exponential indicator variograms—an assumption that is supported by the theory of the transition probability/Markov chain approach (e.g., Carle & Fogg, 1996)—we can postulate that the entropic scale of the K distribution has higher impact on transport than its spatial correlation. This hypothesis will be further discussed in the next section when we consider continuous K fields in which the spatial correlation is precisely defined in terms of integral scale.

4.2. Geological Entropy and Solute Transport: When Good Descriptors of Aquifer Heterogeneity Go Right

The ensemble means of calculated BTCs for the MVN, CNT, and DSC fields are plotted in Figure 4 with two different normalizations of the arrival times. In the panels at the top (Figures 4a and 4b), the particle travel time t is made dimensionless through multiplication with U_h/I where U_h is the flow velocity of a

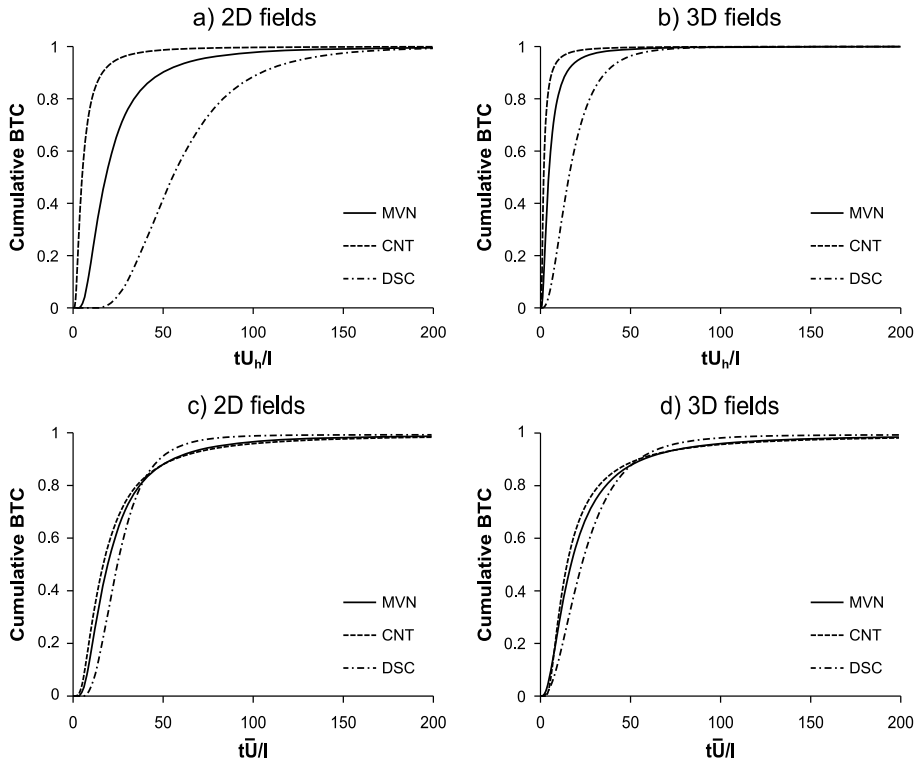

Figure 4. Cumulative breakthrough curves (BTCs) for the different structures in 2-D and 3-D. See the main text for details about the difference in normalization approach of the arrival time (t) in the top (a and b) and bottom panels (c and d). MVN = multivariate normal; CNT = connected; DSC = disconnected.

homogenous aquifer of conductivity equal to K_G (i.e., $U_h = K_G J/\theta$). This type of normalization allows comparisons between our results and those presented in Figure 7 in Zinn and Harvey (2003) and Figure 4 in Jankovic et al. (2017), although in this work we used Gaussian covariance functions for both 2-D and 3-D fields. In the bottom panels (Figures 4c and 4d), the BTCs are shown as function of $t\bar{U}/I$, and therefore, t is normalized by the mean arrival time $\bar{t}$, as in the two previous studies (Figure 8 in Zinn & Harvey, 2003; Figure 3 in Jankovic et al., 2017). Key statistics for the calculated BTCs considering both normalization approaches are also reported in Table 1.

Although the modeling analysis in this work is based on ensemble-averaging over 100 Monte Carlo simulations instead of performing one individual ergodic simulation, the results of the transport simulations match with those by Jankovic et al. (2017), and their main conclusion that the simulated flow and transport are significantly less impacted by the K field structure in 3-D fields compared to 2-D simulations is confirmed. For instance, the early arrival (t_5) expressed in normalized time tU_h/I for 2-D CNT fields is on average about four times faster than in MVN fields. Such difference is reduced by about one half in 3-D fields. Similarly, while the maximum difference in effective K values for 2-D fields is in the order of seven times (DSC versus CNT), a difference by a factor of 5.5 is calculated for 3-D fields. Similar considerations can be formulated for the majority of the parameters in Table 1.

We now show how the entrogram-based analysis can explain these results. The entrograms of the different K and U fields are shown in Figure 5, while the corresponding entropic scales are presented in Table 1 where they are normalized by the integral scales of the K fields. Note that since the CNT fields are generated by simply reflecting the values of the DSC field around the zero ln$K$ mean (Zinn & Harvey, 2003), the two structures are identical in terms of spatial order and therefore their entrograms are overlapped in Figure 5. The higher connectivity in the DSC and CNT structures is reflected by their H_S values, which are about 18% (2-D) and 25% (3-D) higher than the corresponding values for the MVN fields. The comparison of the entrograms and the H_S values between 2-D and 3-D fields indicates that the 2-D structures have a higher degree of spatial order. In particular, the H_S values of the 2-D fields are about 50% and 60% larger for K and U, respectively,

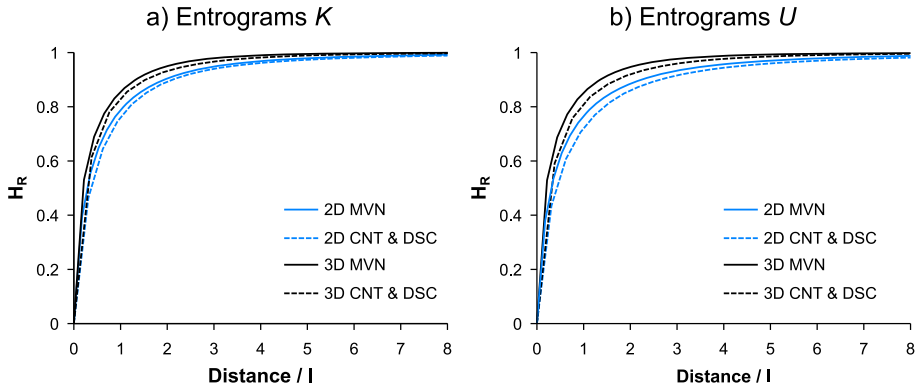

Figure 5. Entrogram comparison for the continuous *K* and Eulerian velocity (*U*) fields. MVN = multivariate normal; CNT = connected; DSC = disconnected.

relative to the corresponding values in 3-D. The lower entropic scales of the 3-D fields can be explained by the introduction of spatial variability in the third dimension and a consequential increment in spatial disorder.

Another result from the entrogram analysis is that the H_S of the *U* fields, both in 2-D and in 3-D, are larger than the corresponding scales for the *K* fields. Previous numerical and theoretical studies (Ababou et al., 1989; Bellin et al., 1992; Gotovac et al., 2009; Salandin & Fiorotto, 1998) have shown that for steady-state flow conditions, the variability of the Eulerian velocity field is reduced compared to that of the corresponding MVN *K* fields, while the correlation length is enhanced. Smaller variability and increased spatial correlation, which in turn increases the degree of spatial order in the structure of the *U* field, is therefore confirmed by the values of the entropic scales. However, while the H_S values of the 2-D *U* fields are about 15% to 22% higher than those of the corresponding *K* fields, this increment in H_S is not as evident for 3-D fields. As such, the entropic scales for *U* and *K* 3-D fields tend to be more similar especially for the MVN structure (about 4% difference between the H_S values for the *U* and *K* fields) while a 7% difference was calculated for the CNT and DSC structures. This analysis can explain the results of the transport simulations shown in Figure 4 and shed light on the different conclusions of Zinn and Harvey (2003) and Jankovic et al. (2017). The different entropic scales for *U* fields in fact indicate that over the entire domain, the persistency of zones with similar flow velocities (e.g., preferential flow paths) is higher for 2-D fields compared to 3-D fields. Consequentially, the impact of fast flow zones on the resulting BTCs, in particular for what concerns their shapes and the corresponding statistics, is more pronounced in 2-D fields than in 3-D fields.

It is also noteworthy that the ratio between the integral scale and the entropic scales of the different *K* fields is in the range between 1.09 to 1.28 for the 2-D fields and between 1.52 to 1.92 for the 3-D fields. We recall that an empirical value around 1.5 was found for the categorical fields as the threshold above which the transport statistics become less significantly impacted by the *K* field structure. Although we cannot compare directly the results from the continuous and categorical fields simulations, there seems to be a consistency in the two examples suggesting that when we compare different *K* field structures, the larger the ratio between a measure of spatial correlation (*I* for the continuous fields; L_h for the categorical fields) and H_S, the lower the impact of the structure on transport. Given that all the analyzed continuous *K* fields have the same *I*, two additional observations can be made: (1) it is confirmed also for continuous *K* field that the entropic scale is a fundamental property of the *K* field controlling transport behavior; (2) because the 2-D and 3-D structures are different in terms of spatial order and geological entropy, they influence solute transport in different ways although they all have the same univariate *K* distribution and covariance function, as well as the same degree of connectivity in some cases (e.g., CNT in 2-D versus CNT in 3-D).

One last factor to consider is the effect of the injection mode (e.g., Demmy et al., 1999; Jankovic & Fiori, 2010; Parker & van Genuchten, 1984) on the entrogram analysis. Our analysis adopts flux-weighted injection, which is more similar to field conditions compared to a uniform (resident) injection. Under flux-weighted injection, a larger number of particles are initially placed in the high-*K* zones compared to the low-K zones; as such, the particle pathlines are not expected to sample the entire *K* and *U* fields. Moreover, particles also tend to

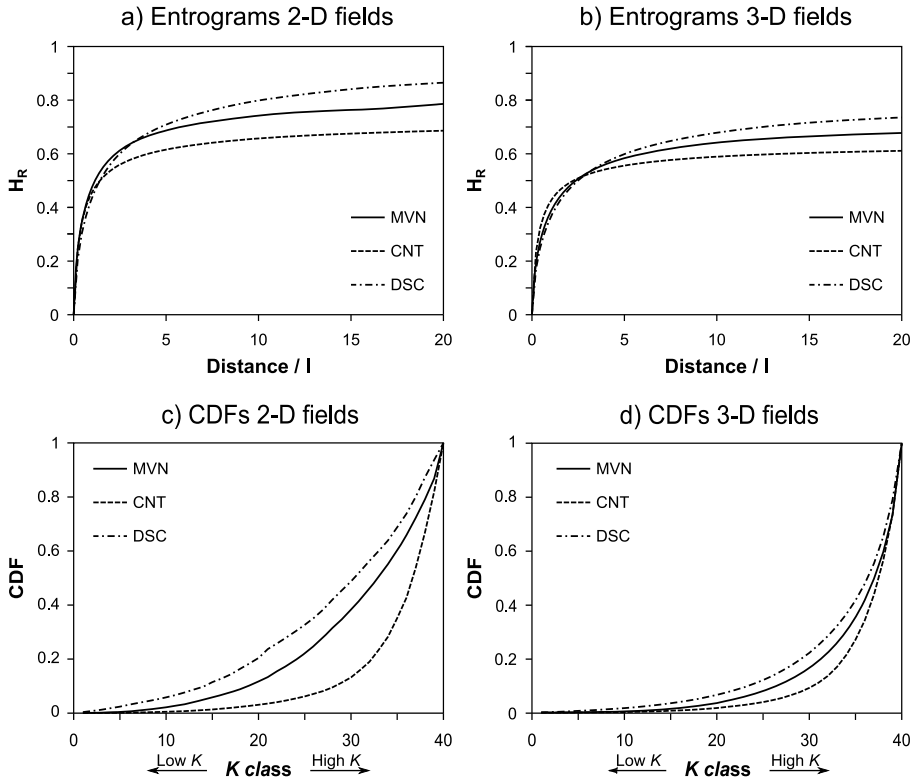

Figure 6. Entrograms of the *K* values intercepted by the particle pathlines in 2-D (a) and 3-D (b) fields and corresponding empirical cumulative distribution functions (CDFs; c and d).

rapidly transition to high-*K* zones and travel within them for relatively long distances (e.g., Bianchi et al., 2011; Le Borgne et al., 2008; Pedretti & Bianchi, 2018) especially if molecular diffusion is not taken into account (LaBolle & Fogg, 2001). In order to consider this bias in the range of *K* values relevant to transport behavior, we first sampled only the *K* values intercepted by the particle paths and then performed the entrogram calculations on these subsamples (Figures 6a and 6b). Two fundamental results of this analysis emerge.

The first result is that by evaluating only the *K* values sampled by the particles, a clear difference is observed between CNT and DSC fields, which was not recognized by the entrograms of the entire *K* and Eulerian *U* fields (Figure 5). This result suggests the existence of "effective" system's entrograms to be associated only to those zones along which transport is actually occurring. Indeed, the "effective" entropic scale is larger for CNT fields than in DSC, consistent with the more structured transport patterns expected in CNT fields.

The second result is that such "effective" entrograms for the considered structures are significantly more similar in 3-D than in 2-D. In particular, the different shapes of the effective entrograms and the generally higher $H_R(l)$ values for the 2-D fields (Figure 6a) indicate that in the 2-D simulations the particles traveled within classes of *K* values with a significantly lower degrees of spatial order compared to the simulations in 3-D. Conversely, the effective entrograms for the 3-D fields (Figure 6b) are more similar regardless of the overall *K* structure (i.e., MVN, CNT, or DSC) indicating not only that particles traveled within comparable ranges of *K* classes but also that the spatial assemblage of these classes have a rather similar degree of spatial order. These observations are further confirmed by the CDFs of the subsamples of *K* values, which show a significantly higher variability for 2-D fields compared to 3-D (Figures 6c and 6d). These results strengthen the knowledge that solutes tend to travel in the upper 15–20% of the *K* distribution (*K* classes 32–40 in Figure 6), which tend to fully percolate in 3-D correlated random fields regardless of their overall structure (Fogg et al., 2000; Fogg & Zhang, 2016; Harter, 2005). In light of these considerations based on the entrogram analysis, it becomes not surprising that the impact of the structures is lower for the 3-D fields relative to the 2-D, which could explain the different conclusions between Zinn and Harvey (2003) and Jankovic et al. (2017).

5. Summary and Conclusions

The geological entropy approach introduced in Bianchi and Pedretti (2017) is expanded in this work with a new tool for spatial analysis called *entrogram*. The entrogram is a variogram-like graph that provides visual assessment of the variability of the relative entropy index H_R at different scales within any type of distributed field. From the entrogram, a metric called *entropic scale* (H_S) can be directly calculated to measure the persistency of patterns of spatial association or clustering and therefore quantify the global degree of spatial order in the spatial distribution. In this work, the entrogram and entropic scale analysis is limited to the assumption of spatial isotropy, but future expansions of these concepts will also include the calculation of directional components to investigate the effects of spatial anisotropy.

The entrogram and entropic scale tools for spatial analysis were applied to investigate the link between aquifer heterogeneity and solute transport in K fields modeled as the distribution of three categories representing hydrofacies in alluvial aquifers. These fields consider a range of mean lengths (L_h) for the most conductive hydrofacies. A clear correlation was found between the entropic scales of these synthetic fields and the results of solute transport simulations. In particular, empirical power-law functions were found to accurately describe the relationships between the L_h/H_S ratio and the statistics of the distributions of the particle arrival times. These expressions mean that in line with the previous findings of Bianchi and Pedretti (2017), transport behavior could be predicted solely from the knowledge of H_S and L_h without requiring a solution of the flow and transport equations. The universal application of these empirical rules requires, however, a clear understanding of the meaning of the best-fitting exponents, a task that remains open for future developments. The results also suggest that there is a threshold, which for the fields considered in this work is in the range 1.5 ± 0.5, above which the considered statistics (with the exception of the skewness) become less sensible to variations in the ratio between the mean length of the hydrofacies and H_S.

Entrograms and entropic scales were also calculated for continuous 2-D and 3-D K field having identical univariate ln$K$ distributions and different connectivity structures. The calculated entrograms and entropic scales were consistent with the expected degrees of spatial order in the considered structures. Detailed numerical experiments similar to those performed by Zinn and Harvey (2003) and Jankovic et al. (2017) emphasized the difference in the impact of the structure of the K field on flow variability and corresponding transport behavior for 2-D and 3-D systems. However, this different impact is explained by the variability of the entrograms and corresponding entropic scales of these structures in 2-D and 3-D, notwithstanding their identical univariate K distributions, covariance functions, and even expected degrees of connectivity. For instance, the entropic scales H_S and the velocity U fields are higher for the 2-D structures compared to the 3-D ones. This result is an indication of higher persistency in 2-D systems of zones with similar flow velocities like preferential flow paths, which in turn influence the distributions of the particle arrival times. Moreover, the entrograms of the K values intercepted by the particle paths for the considered structures are significantly more similar in 3-D than in 2-D. The entrogram analysis indicates that while in 2-D the particles traveled in a different range of classes of conductivity and degree of spatial order for each structure, in 3-D, these differences become less accentuated because in every structure, particles traveled within a narrow range of high-K classes with similar patterns of spatial association. As such, an "effective" entrogram able to predict transport could be associated to the zones of the domain sampled by transport. Exploring this issue in detail is also left open for future development.

Acknowledgments
The authors acknowledge the useful comments and suggestions by the Editor Xavier Sanchez-Vila, Aldo Fiori, and another anonymous reviewer. Marco Bianchi was funded by the Natural Environment Research Council under the "Research Fellowship Programme" of the British Geological Survey. Marco Bianchi publishes with the permission of the Executive Director of the British Geological Survey. Discussions with J. R. Howcroft were useful for the development of the entrogram concept. Constructive comments from B. Marchant also improved an early version of the paper. This is a theoretical work for which no data need be made available.

References

Ababou, R., McLaughlin, D., Gelhar, L. W., & Tompson, A. F. B. (1989). Numerical simulation of three-dimensional saturated flow in randomly heterogeneous porous media. *Transport in Porous Media*, *4*(6), 549–565. https://doi.org/10.1007/BF00223627

Adams, E. E., & Gelhar, L. W. (1992). Field study of dispersion in a heterogeneous aquifer: 2. Spatial moments analysis. *Water Resources Research*, *28*(12), 3293–3307. https://doi.org/10.1029/92WR01757

Anderson, M. P. (1989). Hydrogeologic facies models to delineate large-scale spatial trends in glacial and glaciofluvial sediments. *Geological Society of America Bulletin*, *101*(4), 501–511. https://doi.org/10.1130/0016-7606(1989)

Asher, M. J., Croke, B. F. W., Jakeman, A. J., & Peeters, L. J. M. (2015). A review of surrogate models and their application to groundwater modeling. *Water Resources Research*, *51*, 5957–5973. https://doi.org/10.1002/2015WR016967

Bellin, A., Salandin, P., & Rinaldo, A. (1992). Simulation of dispersion in heterogeneous porous formations: Statistics, first-order theories, convergence of computations. *Water Resources Research*, *28*(9), 2211–2227. https://doi.org/10.1029/92WR00578

Berkowitz, B., Cortis, A., Dentz, M., & Scher, H. (2006). Modeling non-Fickian transport in geological formations as a continuous time random walk. *Reviews of Geophysics*, *44*, RG2003. https://doi.org/10.1029/2005RG000178

Bianchi, M., & Pedretti, D. (2017). Geological entropy and solute transport in heterogeneous porous media. *Water Resources Research*, *53*, 4691–4708. https://doi.org/10.1002/2016WR020195

Bianchi, M., & Zheng, C. (2016). A lithofacies approach for modeling non-Fickian solute transport in a heterogeneous alluvial aquifer. *Water Resources Research*, *52*, 552–565. https://doi.org/10.1002/2015WR018186
Bianchi, M., Zheng, C., Wilson, C., Tick, G. R., Liu, G., & Gorelick, S. M. (2011). Spatial connectivity in a highly heterogeneous aquifer: From cores to preferential flow paths. *Water Resources Research*, *47*, W05524. https://doi.org/10.1029/2009WR008966
Carle, S. F. (1999). *T-PROGS: Transition probability geostatistical software*, (p. 84). Davis, CA: University of California. Retrieved from http://gmsdocs.aquaveo.com/t-progs.pdf
Carle, S. F., & Fogg, G. E. (1996). Transition probability-based indicator geostatistics. *Mathematical Geology*, *28*(4), 453–476. https://doi.org/10.1007/BF02083656
Chiogna, G., Hochstetler, D. L., Bellin, A., Kitanidis, P. K., & Rolle, M. (2012). Mixing, entropy and reactive solute transport. *Geophysical Research Letters*, *39*, L20405. https://doi.org/10.1029/2012GL053295
Cortis, A., & Berkowitz, B. (2004). Anomalous transport in "classical" soil and sand columns. *Soil Science Society of America Journal*, *68*(5), 1539–1548. https://doi.org/10.2136/sssaj2004.1539
Dagan, G. (1989). *Flow and transport in porous formations*. Berlin, Heidelberg: Springer. Retrieved from http://link.springer.com/10.1007/978-3-642-75015-1
Davies, N. S., & Gibling, M. R. (2011). Evolution of fixed-channel alluvial plains in response to Carboniferous vegetation. *Nature Geoscience*, *4*(9), 629–633. https://doi.org/10.1038/ngeo1237
de Barros, F. P. J., Fernàndez-Garcia, D., Bolster, D., & Sanchez-Vila, X. (2013). A risk-based probabilistic framework to estimate the endpoint of remediation: Concentration rebound by rate-limited mass transfer. *Water Resources Research*, *49*, 1929–1942. https://doi.org/10.1002/wrcr.20171
de Marsily, G. (1986). *Quantitative hydrogeology: Groundwater hydrology for engineers*. San Diego: Academic Press.
de Marsily, G., Delay, F., Gonçalvès, J., Renard, P., Teles, V., & Violette, S. (2005). Dealing with spatial heterogeneity. *Hydrogeology Journal*, *13*(1), 161–183. https://doi.org/10.1007/s10040-004-0432-3
Dell'Arciprete, D., Vassena, C., Baratelli, F., Giudici, M., Bersezio, R., & Felletti, F. (2014). Connectivity and single/dual domain transport models: Tests on a point-bar/channel aquifer analogue. *Hydrogeology Journal*, *22*(4), 761–778. https://doi.org/10.1007/s10040-014-1105-5
Demmy, G., Berglund, S., & Graham, W. (1999). Injection mode implications for solute transport in porous media: Analysis in a stochastic Lagrangian framework. *Water Resources Research*, *35*(7), 1965–1973. https://doi.org/10.1029/1999WR900027
Deutsch, C. V., & Journel, A. G. (1998). *GSLIB: geostatistical software library and user's guide*. Oxford, UK: Oxford University Press.
Fernàndez-Garcia, D., Trinchero, P., & Sanchez-Vila, X. (2010). Conditional stochastic mapping of transport connectivity. *Water Resources Research*, *46*, W10515. https://doi.org/10.1029/2009WR008533
Fiori, A. (2014). Channeling, channel density and mass recovery in aquifer transport, with application to the MADE experiment. *Water Resources Research*, *50*, 9148–9161. https://doi.org/10.1002/2014WR015950
Fiori, A., & Jankovic, I. (2012). On preferential flow, channeling and connectivity in heterogeneous porous formations. *Mathematical Geosciences*, *44*(2), 133–145. https://doi.org/10.1007/s11004-011-9365-2
Fiori, A., Zarlenga, A., Gotovac, H., Jankovic, I., Volpi, E., Cvetkovic, V., & Dagan, G. (2015). Advective transport in heterogeneous aquifers: Are proxy models predictive? *Water Resources Research*, *51*, 9577–9594. https://doi.org/10.1002/2015WR017118
Fiori, A., Zarlenga, A., Jankovic, I., & Dagan, G. (2017). Solute transport in aquifers: The comeback of the advection dispersion equation and the first order approximation. *Advances in Water Resources*, *110*, 349–359. https://doi.org/10.1016/j.advwatres.2017.10.025
Fogg, G. E. (1986). Groundwater flow and sand body interconnectedness in a thick, multiple-aquifer system. *Water Resources Research*, *22*(5), 679–694. https://doi.org/10.1029/WR022i005p00679
Fogg, G. E., Carle, S. F., & Green, C. (2000). Connected-network paradigm for the alluvial aquifer system. *Geological Society of America Special Papers*, *348*, 25–42. https://doi.org/10.1130/0-8137-2348-5.25
Fogg, G. E., & Zhang, Y. (2016). Debates—Stochastic subsurface hydrology from theory to practice: A geologic perspective. *Water Resources Research*, *52*, 9235–9245. https://doi.org/10.1002/2016WR019699
Freixas, G., Fernàndez-Garcia, D., & Sanchez-Vila, X. (2017). Stochastic estimation of hydraulic transmissivity fields using flow connectivity indicator data. *Water Resources Research*, *53*, 602–618. https://doi.org/10.1002/2015WR018507
Gelhar, L. W. (1993). *Stochastic subsurface hydrology*. Upper Saddle River, NJ: Prentice-Hall.
Gómez-Hernández, J. J., & Wen, X.-H. (1998). To be or not to be multi-Gaussian? A reflection on stochastic hydrogeology. *Advances in Water Resources*, *21*(1), 47–61. https://doi.org/10.1016/S0309-1708(96)00031-0
Gotovac, H., Cvetkovic, V., & Andricevic, R. (2009). Flow and travel time statistics in highly heterogeneous porous media. *Water Resources Research*, *45*, W07402. https://doi.org/10.1029/2008WR007168
Haggerty, R., & Gorelick, S. M. (1995). Multiple-rate mass transfer for modeling diffusion and surface reactions in media with pore-scale heterogeneity. *Water Resources Research*, *31*(10), 2383–2400. https://doi.org/10.1029/95WR10583
Harbaugh, A. W. (2005). MODFLOW-2005, the U.S. Geological survey modular ground-water model—The ground-water flow process.
Harter, T. (2005). Finite-size scaling analysis of percolation in three-dimensional correlated binary Markov chain random fields. *Physical Review E*, *72*(2), 026120. https://doi.org/10.1103/PhysRevE.72.026120
Hunt, A. G., & Sahimi, M. (2017). Flow, transport, and reaction in porous media: Percolation scaling, critical-path analysis, and effective medium approximation. *Reviews of Geophysics*, *55*(4), 993–1078. https://doi.org/10.1002/2017RG000558
Isaaks, E. H., & Srivastava, R. M. (1990). *Applied geostatistics*. New York, NY: OUP USA.
Jankovic, I., & Fiori, A. (2010). Analysis of the impact of injection mode in transport through strongly heterogeneous aquifers. *Advances in Water Resources*, *33*(10), 1199–1205. https://doi.org/10.1016/j.advwatres.2010.05.006
Jankovic, I., Maghrebi, M., Fiori, A., & Dagan, G. (2017). When good statistical models of aquifer heterogeneity go right: The impact of aquifer permeability structures on 3D flow and transport. *Advances in Water Resources*, *100*, 199–211. https://doi.org/10.1016/j.advwatres.2016.10.024
Journel, A. G., & Deutsch, C. V. (1993). Entropy and spatial disorder. *Mathematical Geology*, *25*(3), 329–355. https://doi.org/10.1007/BF00901422
Kang, P. K., Dentz, M., Le Borgne, T., Lee, S., & Juanes, R. (2017). Anomalous transport in disordered fracture networks: Spatial Markov model for dispersion with variable injection modes. *Advances in Water Resources*, *106*, 80–94. https://doi.org/10.1016/j.advwatres.2017.03.024
Kitanidis, P. K. (1994). The concept of the dilution index. *Water Resources Research*, *30*(7), 2011–2026. https://doi.org/10.1029/94WR00762
Knudby, C., & Carrera, J. (2005). On the relationship between indicators of geostatistical, flow and transport connectivity. *Advances in Water Resources*, *28*(4), 405–421. https://doi.org/10.1016/j.advwatres.2004.09.001
Knudby, C., & Carrera, J. (2006). On the use of apparent hydraulic diffusivity as an indicator of connectivity. *Journal of Hydrology*, *329*(3–4), 377–389. https://doi.org/10.1016/j.jhydrol.2006.02.026
LaBolle, E. M., & Fogg, G. E. (2001). Role of molecular diffusion in contaminant migration and recovery in an alluvial aquifer system. *Transport in Porous Media*, *42*(1/2), 155–179. https://doi.org/10.1023/A:1006772716244

Le Borgne, T., Dentz, M., & Carrera, J. (2008). Spatial Markov processes for modeling Lagrangian particle dynamics in heterogeneous porous media. *Physical Review E*, *78*(2), 26308. https://doi.org/10.1103/PhysRevE.78.026308

Lee, S.-Y., Carle, S. F., & Fogg, G. E. (2007). Geologic heterogeneity and a comparison of two geostatistical models: Sequential Gaussian and transition probability-based geostatistical simulation. *Advances in Water Resources*, *30*(9), 1914–1932. https://doi.org/10.1016/j.advwatres.2007.03.005

Liu, G., Zheng, C., & Gorelick, S. M. (2004). Limits of applicability of the advection-dispersion model in aquifers containing connected high-conductivity channels. *Water Resources Research*, *40*, W08308. https://doi.org/10.1029/2003WR002735

Matheron, G. (1967). Elements pour une théorie des milieux poreux. Retrieved from https://infoscience.epfl.ch/record/27350

Maxwell, R. M., Carle, S. F., & Tompson, A. F. B. (2008). Contamination, risk, and heterogeneity: on the effectiveness of aquifer remediation. *Environmental Geology*, *54*(8), 1771–1786. https://doi.org/10.1007/s00254-007-0955-8

Mays, D. C., Faybishenko, B. A., & Finsterle, S. (2002). Information entropy to measure temporal and spatial complexity of unsaturated flow in heterogeneous media. *Water Resources Research*, *38*(12), 49-1–49–11. https://doi.org/10.1029/2001WR001185

Molinari, A., Pedretti, D., & Fallico, C. (2015). Analysis of convergent flow tracer tests in a heterogeneous sandy box with connected gravel channels. *Water Resources Research*, *51*(7), 5640–5657. https://doi.org/10.1002/2014WR016216

Naimi, N. (2015). On uncertainty in species distribution modelling. doi: https://doi.org/10.3990/1.9789036538404

Neuman, S. P., & Tartakovsky, D. M. (2009). Perspective on theories of non-Fickian transport in heterogeneous media. *Advances in Water Resources*, *32*(5), 670–680. https://doi.org/10.1016/j.advwatres.2008.08.005

Neuman, S. P., Winter, C. L., & Newman, C. M. (1987). Stochastic theory of field-scale Fickian dispersion in anisotropic porous media. *Water Resources Research*, *23*(3), 453–466. https://doi.org/10.1029/WR023i003p00453

Parker, J. C., & van Genuchten, M. T. (1984). Flux-averaged and volume-averaged concentrations in continuum approaches to solute transport. *Water Resources Research*, *20*(7), 866–872. https://doi.org/10.1029/WR020i007p00866

Pedretti, D., & Bianchi, M. (2018). Reproducing tailing in breakthrough curves: Are statistical models equally representative and predictive? *Advances in Water Resources*, *113*, 236–248. https://doi.org/10.1016/j.advwatres.2018.01.023

Pollock, D. W. (2016). User guide for MODPATH version 7—A particle-tracking model for MODFLOW. U.S. Geological Survey Open-File Report No. 2016-1086 (p. 35).

Refsgaard, J. C., van der Sluijs, J. P., Brown, J., & van der Keur, P. (2006). A framework for dealing with uncertainty due to model structure error. *Advances in Water Resources*, *29*(11), 1586–1597. https://doi.org/10.1016/j.advwatres.2005.11.013

Rehfeldt, K. R., Boggs, J. M., & Gelhar, L. W. (1992). Field study of dispersion in a heterogeneous aquifer: 3. Geostatistical analysis of hydraulic conductivity. *Water Resources Research*, *28*(12), 3309–3324. https://doi.org/10.1029/92WR01758

Remy, N., Boucher, A., & Wu, J. (2009). *Applied geostatistics with SGeMS: A user's guide*, (1st ed.). Cambridge, UK: Cambridge University Press. https://doi.org/10.1017/CBO9781139150019

Renard, P., & Allard, D. (2013). Connectivity metrics for subsurface flow and transport. *Advances in Water Resources*, *51*, 168–196. https://doi.org/10.1016/j.advwatres.2011.12.001

Rizzo, C. B., & de Barros, F. P. J. (2017). Minimum hydraulic resistance and least resistance path in heterogeneous porous media. *Water Resources Research*, *53*, 8596–8613. https://doi.org/10.1002/2017WR020418

Rubin, Y. (2003). *Applied Stochastic Hydrogeology*. Oxford, UK: Oxford University Press.

Rubin, Y., & Seong, K. (1994). Investigation of flow and transport in certain cases of nonstationary conductivity fields. *Water Resources Research*, *30*(11), 2901–2911. https://doi.org/10.1029/94WR01950

Salamon, P., Fernàndez-Garcia, D., & Gómez-Hernández, J. J. (2006). Modeling mass transfer processes using random walk particle tracking. *Water Resources Research*, *42*, W11417. https://doi.org/10.1029/2006WR004927

Salandin, P., & Fiorotto, V. (1998). Solute transport in highly heterogeneous aquifers. *Water Resources Research*, *34*(5), 949–961. https://doi.org/10.1029/98WR00219

Sánchez-Vila, X., Carrera, J., & Girardi, J. P. (1996). Scale effects in transmissivity. *Journal of Hydrology*, *183*(1), 1–22. https://doi.org/10.1016/S0022-1694(96)80031-X

Sanchez-Vila, X., & Fernàndez-Garcia, D. (2016). Debates-stochastic subsurface hydrology from theory to practice: Why stochastic modeling has not yet permeated into practitioners? *Water Resources Research*, *52*, 9246–9258. https://doi.org/10.1002/2016WR019302

Sanchez-Vila, X., Guadagnini, A., & Carrera, J. (2006). Representative hydraulic conductivities in saturated groundwater flow. *Reviews of Geophysics*, *44*, RG3002. https://doi.org/10.1029/2005RG000169

Shannon, C. E. (1948). A mathematical theory of communication. *Bell System Technical Journal*, *27*(3), 379–423. https://doi.org/10.1002/j.1538-7305.1948.tb01338.x

Stauffer, D., & Aharony, A. (1994). *Introduction to percolation theory*, (Revised Second ed.p. 181). Boca Raton, FL: CRC Press.

Tompson, A. F. B., Falgout, R. D., Smith, S. G., Bosl, W. J., & Ashby, S. F. (1998). Analysis of subsurface contaminant migration and remediation using high performance computing. *Advances in Water Resources*, *22*(3), 203–221. https://doi.org/10.1016/S0309-1708(98)00013-X

Trinchero, P., Sánchez-Vila, X., & Fernàndez-Garcia, D. (2008). Point-to-point connectivity, an abstract concept or a key issue for risk assessment studies? *Advances in Water Resources*, *31*(12), 1742–1753. https://doi.org/10.1016/j.advwatres.2008.09.001

Tyukhova, A. R., & Willmann, M. (2016a). Connectivity metrics based on the path of smallest resistance. *Advances in Water Resources*, *88*, 14–20. https://doi.org/10.1016/j.advwatres.2015.11.014

Tyukhova, A. R., & Willmann, M. (2016b). Conservative transport upscaling based on information of connectivity: Transport upscaling using connectivity. *Water Resources Research*, *52*, 6867–6880. https://doi.org/10.1002/2015WR018331

Weissmann, G. S., Carle, S. F., & Fogg, G. E. (1999). Three-dimensional hydrofacies modeling based on soil surveys and transition probability geostatistics. *Water Resources Research*, *35*(6), 1761–1770. https://doi.org/10.1029/1999WR900048

Wen, X.-H., & Gómez-Hernández, J. J. (1996). Upscaling hydraulic conductivities in heterogeneous media: An overview. *Journal of Hydrology*, *183*(1–2), ix–xxxii. https://doi.org/10.1016/S0022-1694(96)80030-8

Wen, X.-H., & Gómez-Hernández, J. J. (1998). Numerical modeling of macrodispersion in heterogeneous media: A comparison of multi-Gaussian and non-multi-Gaussian models. *Journal of Contaminant Hydrology*, *30*(1-2), 129–156. https://doi.org/10.1016/S0169-7722(97)00035-1

Willmann, M., Carrera, J., & Sánchez-Vila, X. (2008). Transport upscaling in heterogeneous aquifers: What physical parameters control memory functions? *Water Resources Research*, *44*, W12437. https://doi.org/10.1029/2007WR006531

Ye, Y., Chiogna, G., Lu, C., & Rolle, M. (2017). Effect of anisotropy structure on plume entropy and reactive mixing in helical flows. *Transport in Porous Media*, *121*(2), 315–332. https://doi.org/10.1007/s11242-017-0964-3

Zhang, Y., Benson, D. A., & Baeumer, B. (2007). Predicting the tails of breakthrough curves in regional-scale alluvial systems. *Ground Water*, *45*(4), 473–484. https://doi.org/10.1111/j.1745-6584.2007.00320.x

Zheng, C., Bianchi, M., & Gorelick, S. M. (2011). Lessons learned from 25 years of research at the MADE site. *Ground Water*, *49*(5), 649–662. https://doi.org/10.1111/j.1745-6584.2010.00753.x

Zheng, C., & Gorelick, S. M. (2003). Analysis of solute transport in flow fields influenced by preferential flowpaths at the decimeter scale. *Ground Water*, *41*(2), 142–155. https://doi.org/10.1111/j.1745-6584.2003.tb02578.x

Zinn, B., & Harvey, C. F. (2003). When good statistical models of aquifer heterogeneity go bad: A comparison of flow, dispersion, and mass transfer in connected and multivariate Gaussian hydraulic conductivity fields. *Water Resources Research*, *39*(3), 1051. https://doi.org/10.1029/2001WR001146